Liquid Crystals
Publication details, including instructions for authors and subscription information:
http://www.informaworld.com/smpp/title~content=t713926090

On the parabolic cyclide focal-conic defect in smectic liquid crystals

I. W. Stewart[a]
[a] Department of Theoretical Mechanics, University of Nottingham, Nottingham, England

To cite this Article Stewart, I. W.(1993) 'On the parabolic cyclide focal-conic defect in smectic liquid crystals', Liquid Crystals, 15: 6, 859 — 869
To link to this Article: DOI: 10.1080/02678299308036505
URL: http://dx.doi.org/10.1080/02678299308036505

LIQUID CRYSTALS, 1993, VOL. 15, NO. 6, 859–869

On the parabolic cyclide focal-conic defect in smectic liquid crystals

by I. W. STEWART
Department of Theoretical Mechanics, University of Nottingham, University Park, Nottingham NG7 2RD, England

(*Received 18 May 1993; accepted 22 June 1993*)

This article demonstrates how parallel equidistant layers of parabolic cyclides can be fitted together theoretically to achieve the layering configurations of the experiments reported in the smectic liquid crystal literature. The mathematical construction of the cylide layers is based on two confocal parabolas which correspond to the physical presence of focal-conic line defects in smectic liquid crystals. Suitable parameterizations of the cyclide surfaces allow the relationship between the layers and these parabolic defects to be presented in three-dimensional plots which show cross-sections of the layers near the defects. The results presented are discussed in relation to the static solutions of smectic continuum theory and experimental observations.

1. Introduction

There has recently been considerable interest in the focal-conic structure of smectic C liquid crystals. There are two main types of focal-conic defect which are relevant to smectics, namely, the well-known Dupin cyclide as discussed, for example, in [1–7], and the less familiar parabolic cyclide, examined and depicted in [4, 6, 8–11]. The geometrical construction of a cyclide is dependent upon a pair of confocal-conics. From Dupin's definition it can be derived that cyclides are surfaces which are simultaneously the envelopes of two one parameter families of spheres whose centres lie along a pair of mutually perpendicular focal-conics. The Dupin cyclide has its structure based upon an ellipse and a hyperbola in mutually perpendicular planes, one branch of the hyperbola passing through a focus of the ellipse. The parabolic cyclide is constructed from two confocal-parabolas in perpendicular planes, each parabola passing through the focus of the other. Cyclides can be difficult to visualize: a convenient summary and pictures of such surfaces and their construction may be found in Hirst [11] or Hilbert and Cohn-Vossen [12]. It is the aim of this article to show how parallel layers of parabolic cyclides may be built up in three dimensions. The corresponding structure for Dupin cyclides is already well documented in [1–5, 7], but in all the references to parabolic cyclides only one individual layer [6, 8, 9] or two-dimensional cross-sections of layers [4, 8, 10] have been pictured; although the three-dimensional parallel layering of parabolic cyclides has been discussed in [8, 13], the structure had not been depicted. Three-dimensional plots of multiple layers will be presented in this article. The reason such plots have not been given before is that there seems to be a lack of a suitable parameterization of the cyclide surfaces. This problem, as shown below, may be overcome by employing the parameterization presented in [9, 14]. It is then possible to visualize the internal layering structure for smectics in parabolic cyclide configurations.

The plan of this article is as follows. Section 2 briefly summarizes the static equilibrium solutions for parabolic cyclides in smectic liquid crystals which have

0267-8292/93 $10·00

recently been presented in [9, 14] using smectic continuum theory. Section 3 examines and portrays graphically the internal layering structure for parabolic cyclide layers, the crucial parameterization being given by equation (3.4) below. The relationship with experimental observations is also mentioned. The article concludes with a discussion in § 4.

2. Equilibrium solutions for parabolic cyclides

We begin with a brief mathematical description of smectic liquid crystals. Liquid crystals consist of elongated molecules for which the molecular long axes locally adopt one common direction in space, generally described by a unit vector **n** called the director. Smectic C liquid crystals are layered structures where the director **n** makes an angle θ with respect to the layer normal. The unit vector **a**, the layer normal, is used to describe the equidistant parallel layer structure of smectics. Away from dislocations we must have [15]

$$\nabla \wedge \mathbf{a} = \mathbf{0}. \tag{2.1}$$

As in de Gennes [3], a unit vector **c** is introduced which is perpendicular to **a** and is the unit orthogonal projection of the director **n** on to the smectic planes: **c** is always tangential to the smectic layers. The two directors **a** and **c** are consequently subject to the further constraints

$$\mathbf{a} \cdot \mathbf{a} = \mathbf{c} \cdot \mathbf{c} = 1, \quad \mathbf{a} \cdot \mathbf{c} = 0. \tag{2.2}$$

Knowledge of **a** and **c** completely describes the smectic alignment. A bulk energy integrand based on **a** and **c** and their gradients can be constructed, namely [16],

$$\begin{aligned} 2W = {} & K_1(\nabla \cdot \mathbf{a})^2 + K_2(\nabla \cdot \mathbf{c})^2 + K_3(\mathbf{a} \cdot \nabla \wedge \mathbf{c})^2 + K_4(\mathbf{c} \cdot \nabla \wedge \mathbf{c})^2 \\ & + K_5(\mathbf{b} \cdot \nabla \wedge \mathbf{c})^2 + 2K_6(\nabla \cdot \mathbf{a})(\mathbf{b} \cdot \nabla \wedge \mathbf{c}) + 2K_7(\mathbf{a} \cdot \nabla \wedge \mathbf{c})(\mathbf{c} \cdot \nabla \wedge \mathbf{c}) \\ & + 2K_8(\nabla \cdot \mathbf{c})(\mathbf{b} \cdot \nabla \wedge \mathbf{c}) + 2K_9(\nabla \cdot \mathbf{a})(\nabla \cdot \mathbf{c}) \end{aligned} \tag{2.3}$$

where the K_is are elastic constants and $\mathbf{b} = \mathbf{a} \wedge \mathbf{c}$. These elastic constants are related to those introduced by the Orsay Group [17], as demonstrated in [16]. Using the continuum theory introduced in [14], minimizing this energy leads to two coupled sets of Euler–Lagrange equations, one set for **a** and the other for **c**. These equations contain four Lagrange multipliers on account of the four constraints contained in (2.1) and (2.2). The key to finding cyclide solutions to the equilibrium equations is to transform the equations to a more suitable coordinate system. Stewart *et al.* [9], successfully transformed to a local orthogonal frame for the parabolic cyclides denoted $\{\hat{\boldsymbol{\mu}}, \hat{\boldsymbol{\vartheta}}, \hat{\mathbf{t}}\}$, where $\hat{\boldsymbol{\mu}}$ is the unit layer normal to the cyclide surface and $\hat{\boldsymbol{\vartheta}}$ and $\hat{\mathbf{t}}$ are local unit orthogonal vectors tangential to the cyclide surface (see § 3 below). Solutions to the transformed versions of the Euler–Lagrange equations for a restricted energy only containing the six terms K_1 to K_6 were found in [9], namely

$$\mathbf{a} = \hat{\boldsymbol{\mu}}, \quad \mathbf{c} = \hat{\boldsymbol{\vartheta}}. \tag{2.4}$$

The four Lagrange multipliers necessary for the solution of the equilibrium equations were also derived explicitly. It can be checked directly that the solutions (2.4) satisfy constraints (2.1) and (2.2); for full mathematical details of these solutions the reader is referred to [9]. Of course, the solutions (2.4) are not defined on the conics themselves, which appear as line defects. (A similar approach has been adopted by Nakagawa [7] in his solutions for Dupin cyclides for the same six term version of the energy.) It turns out

that the parameterization required to find static solutions also allows us mathematically to construct and understand the parabolic cyclide layer structure, as will be discussed in the remainder of this article. Although this parameterization arose from examining non-chiral smectic C phases, it is expected that the geometrical structure of the layering will be the same for the smectic A and ferroelectric chiral smectic C* phases.

3. Layers of parabolic cyclides in three dimensions

The cartesian equation of a parabolic cyclide can be conveniently written as [9, 11, 14]

$$x(x^2+y^2+z^2)+(x^2+y^2)(\ell-\mu)-z^2(\ell+\mu)-(x-\mu+\ell)(\ell+\mu)^2=0, \tag{3.1}$$

where the confocal-parabolas in mutually perpendicular planes essential to the construction of the cyclide are

$$y^2=4\ell(x+\ell), \quad z=0, \tag{3.2}$$

and

$$z^2=-4\ell x, \quad y=0. \tag{3.3}$$

Here ℓ and μ are real parameters, -4ℓ being the latus rectum of parabola (3.3). We shall always assume that $\ell\neq 0$. As shown in [9], varying μ provides parallel families of parabolic cyclides. Equation (3.1) may be parameterized as [9, 14]

$$\left.\begin{aligned} x&=\{\mu(\vartheta^2+t^2-1)+\ell(t^2-\vartheta^2-1)\}(1+\vartheta^2+t^2)^{-1},\\ y&=2t(\ell(\vartheta^2+1)+\mu)(1+\vartheta^2+t^2)^{-1},\\ z&=2\vartheta(\ell t^2-\mu)(1+\vartheta^2+t^2)^{-1}, \end{aligned}\right\} \tag{3.4}$$

where

$$\left.\begin{aligned} -\infty<\mu<+\infty,\\ -\infty<\vartheta<+\infty,\\ -\infty<t<+\infty. \end{aligned}\right\} \tag{3.5}$$

For fixed μ, varying ϑ and t maps out one complete cyclide surface. Continuing this process for different fixed values of μ gives parallel layers of cyclides (equidistant if μ changes by the same amount, for example, $\mu=\ldots-2,-1,0,1,2,\ldots$, etc). The parabolas (3.2) and (3.3) become, respectively,

$$t^2=\mu/\ell, \quad z=0 \tag{3.6}$$

and

$$\vartheta^2=-(\mu+\ell)/\ell, \quad y=0. \tag{3.7}$$

It can be checked directly that the parameterization (3.4) satisfies the cartesian equation (3.1). (It should be mentioned that Forsyth [18] has developed a similar parameterization which unfortunately contains errors.)

To illustrate how layers are built up in smectic liquid crystals, we first note that there are three possible types of parabolic cyclide surface, depending on the relative signs and sizes of μ and ℓ. For example, it will be shown below that if $\ell<0$ then for $0<\mu<-\ell$ there are cyclides of the form depicted in figure 1 (where $\ell=-4$, and $\mu=1$).

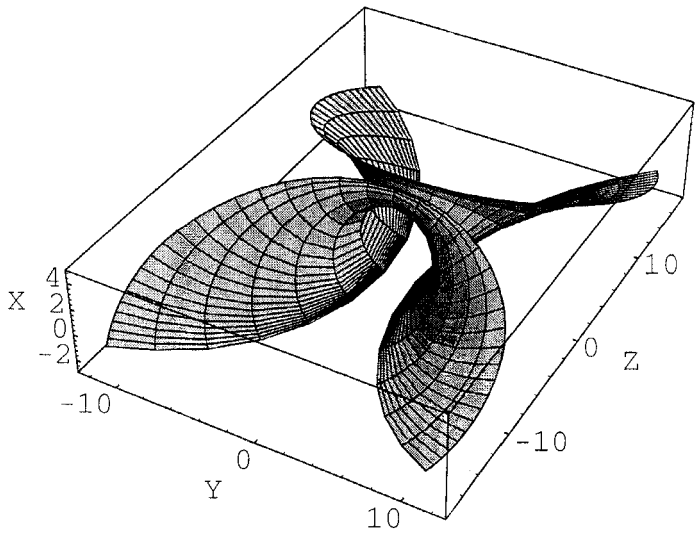

Figure 1. The parabolic cyclide when $\ell = -4$ and $\mu = 1$ plotted for the ranges $-3 \leqslant \vartheta \leqslant 3$ and $-5 \leqslant t \leqslant 5$.

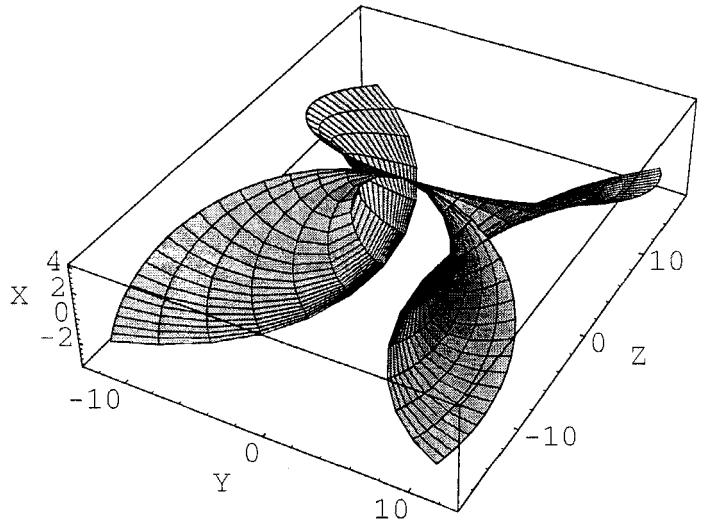

Figure 2. A cusp appears when $\mu = 0$. Here $\ell = -4$ and $-3 \leqslant \vartheta \leqslant 3$ with $-5 \leqslant t \leqslant 5$.

When $\mu = 0$, a cusp point appears for any $\ell \neq 0$ as shown in figure 2, while $\ell < 0$ with $\mu < 0$ gives rise to the form pictured in figure 3 (where $\ell = -4$ and $\mu = -1$) which has a 'bridge' joining two cusp points lying on the parabola (3.6) in the xy-plane. Figure 2 is really a special case of figure 3, when the cusp points coincide at the vertex of parabola (3.6). Since we are principally interested in the defects near the foci of the parabolas, these surfaces are only plotted for $-3 \leqslant \vartheta \leqslant 3$ and $-5 \leqslant t \leqslant 5$ using equations (3.4), the complete surfaces being drawn if ϑ and t are allowed to tend to $\pm\infty$. As noted by Rosenblatt *et al.* [8], the bridge part of the surface in figure 3 has no physical interpretation for liquid crystals: omitting this bridge has no consequence on the mathematical static equilibrium solutions derived in [9], since solutions exist

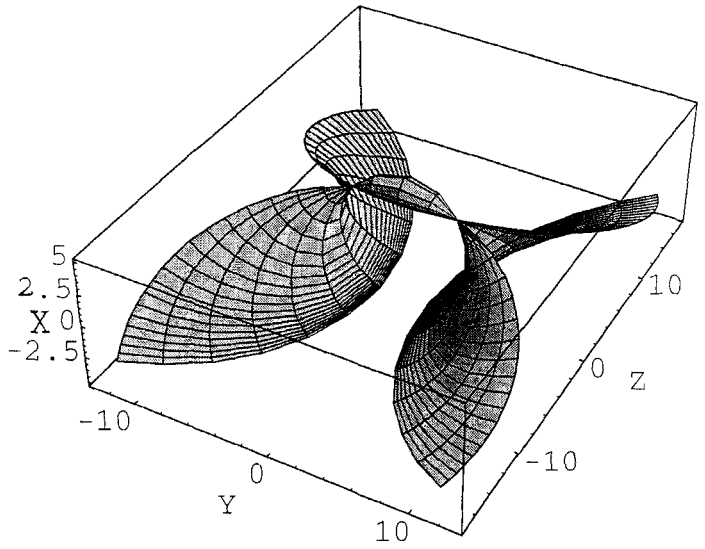

Figure 3. Bridges appear for $\ell < \mu < 0$. In this case $\ell = -4$, $\mu = -1$ and $-3 \leqslant \vartheta \leqslant 3$ with $-5 \leqslant t \leqslant 5$.

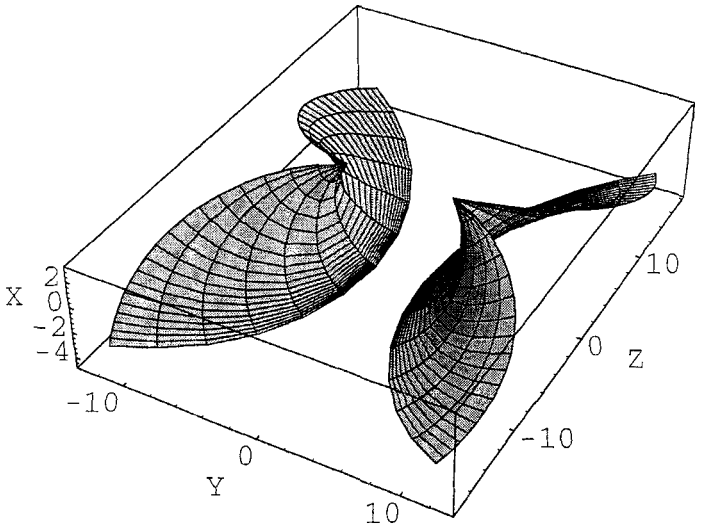

Figure 4. This is figure 3 with the bridge omitted: $\ell = -4$, $\mu = -1$ and the plot is for the ranges $-3 \leqslant \vartheta \leqslant 3$ with $-5 \leqslant t \leqslant -1/2$ and $1/2 \leqslant t \leqslant 5$. The bridge can only appear when $-1/2 < t < 1/2$.

everywhere on the cyclide surface except at the cusp points on the parabola at each side of the bridge. We will demonstrate that omitting bridges (by suitably selecting the correct ranges for parameterization) will allow us to examine the three-dimensional equidistant layering of the cyclides. Figure 4 shows figure 3 without the bridge.

For simplicity we shall always assume that ℓ is fixed and $\ell < 0$; the $\ell > 0$ case is similar except for changes in signs of μ. The reason for choosing $\ell < 0$ is that for small positive values of μ we then have surfaces without defects as shown in figure 1, while small negative values of μ give surfaces with defects as in figure 3: this leads to the

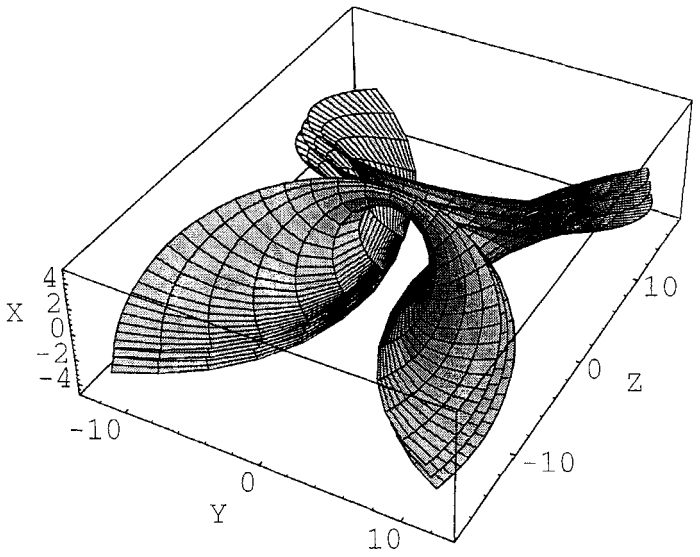

Figure 5. Combining figures 1, 2 and 4 for $\mu = -1, 0, 1$ yields this plot showing how parallel layers fit together. The other parameters and ranges are as in the relevant preceeding figures.

convention of positivity in μ for no defects and negativity in μ for defects near the foci of the parabolas, where our main interest lies. In fact, there are always defects for $\ell < 0$ whenever $\mu \geqslant -\ell$ or $\mu \leqslant 0$: for $\mu \leqslant 0$ the defects are on parabola (3.6), while for $\mu \geqslant -\ell$ they lie on parabola (3.7). When $\mu < 0$ bridges based on parabola (3.6) appear for $-\sqrt{(\mu/\ell)} < t < \sqrt{(\mu/\ell)}$ and when $\mu > -\ell$ bridges appear on parabola (3.7) for $-\sqrt{[-(\mu+\ell)/\ell]} < \vartheta < \sqrt{[-(\mu+\ell)/\ell]}$. Figure 5 shows three parallel layers built up for the cases $\ell = -4$ and $\mu = -1, 0$, and 1, ϑ and t having the same ranges as in figures 1 and 2, except for the $\mu = -1$ case where, to omit the bridge, we must only take $-5 \leqslant t \leqslant -1/2$ and $1/2 \leqslant t \leqslant 5$ (the bridge appears whenever $-1/2 < t < 1/2$). Figure 5 is obtained simply by combining figures 1, 2 and 4 together. We can of course build up more layers, but the plots become difficult to interpret and the internal layering structure will always be hidden (bridges also start appearing on the parabola (3.7) for $\mu > -\ell$, as shown below). For this reason we proceed to take slices through coordinate planes to show the internal structure. As in Hartshorne and Stuart [5], who discussed the Dupin cyclide, we shall examine cuts through the two planes containing the focal-conics, the remaining structure being clear from the symmetry and the three-dimensional plots.

3.1. *The $z = 0$ plane*

When $z = 0$, there is a line defect on parabola (3.6) in the xy-plane and we must, by (3.4), have one of the following possibilities:

$$\text{(i) } \vartheta = 0, \quad \text{(ii) } \vartheta = \pm\infty, \quad \text{(iii) } t^2 = \mu/\ell. \tag{3.8}$$

For $\mu \geqslant 0$, only (3.8) (i) and (ii) are relevant since $\ell < 0$. In case (3.8) (i) we have from (3.4)

$$\left.\begin{aligned} x &= (t^2-1)(\ell+\mu)(t^2+1)^{-1}, \\ y &= 2t(\ell+\mu)(t^2+1)^{-1}. \end{aligned}\right\} \tag{3.9}$$

Clearly

$$x^2+y^2=(\ell+\mu)^2 \tag{3.10}$$

and therefore for $0\leqslant\mu\leqslant-\ell$, we have complete circles in the xy-plane parameterized by (3.9) for $-\infty<t<+\infty$ centred at $(0,0,0)$ and of radius $|\ell+\mu|$. At $\mu=-\ell$ we arrive at parabola (3.7) and bridges start appearing whose cusp points lie outside the $z=0$ plane for $\mu>-\ell$ (and so do not appear in figure 6 below, since we assume that bridges can be ignored from physical considerations). Further, from case (3.8) (ii) and (3.4), we have to include the straight lines

$$x=\mu-\ell,\quad y=2t\ell,\quad z=0,\quad -\infty<t<+\infty, \tag{3.11}$$

whenever $\mu\geqslant0$. Equations (3.10) and (3.11) complete the description of cross-sections of layers as we vary μ in the $z=0$ plane for $0\leqslant\mu<+\infty$: we have circles for $0\leqslant\mu\leqslant-\ell$, together with straight lines for $\mu\geqslant0$. For the situation when $\mu<0$, equation (3.8) (iii) is possible: at $\mu=0$ bridges start appearing on parabola (3.6). Again, both equations (3.9) and (3.11) still hold, the only difference being that to avoid bridges we must parameterize these equations only for the regions $-\infty<t\leqslant-\sqrt{(\mu/\ell)}$ and $\sqrt{(\mu/\ell)}\leqslant t<+\infty$. Figure 6 shows the resulting cross-section in the xy-plane when $z=0$ for the case $\ell=-4$ and μ ranges from -7 to 11 in steps of 1. For simplicity the maximum and minimum values for t have been taken to be 2 and -2. The parabolic line defect corresponding to (3.6) is clearly visible and figure 6 matches the experimental observations depicted in Gray and Goodby [4], Rosenblatt *et al.* [8], and Benton and Miller [10].

To observe the internal three-dimensional structure of the layering near $z=0$ we can plot the cyclides using (3.4) and consider $\vartheta\leqslant0$, effectively cutting the family of cyclides in two along the $z=0$ plane. The resulting layers are shown in figure 7, where $\ell=-4$ and $\mu=-2,-1,0,1,2,3,4,5,6$. For $0\leqslant\mu\leqslant4$, we have plotted equations (3.4) for $-3\leqslant\vartheta\leqslant0$ and $-5\leqslant t\leqslant5$. To avoid bridges on parabola (3.6) for $\mu=-2,-1$, we

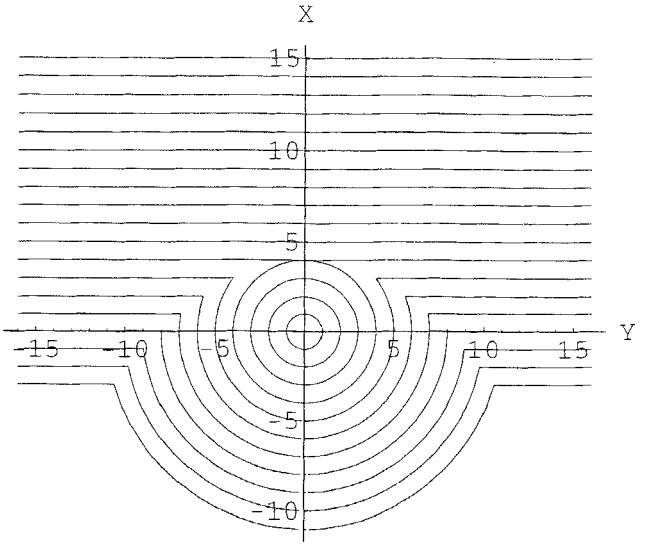

Figure 6. The cross-section of the layers in the xy-plane when $\ell=-4$ and μ ranges from -7 to 11 in steps of 1. The parabolic defect (3.2) (or, equivalently, (3.6)) is clearly visible.

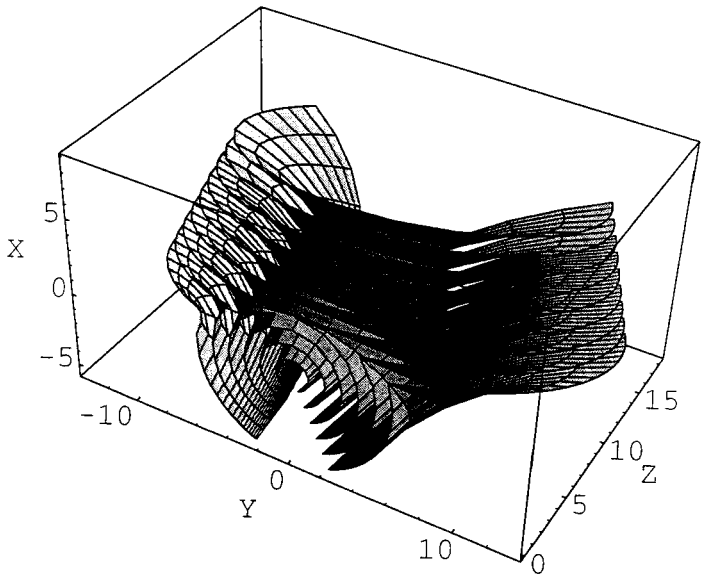

Figure 7. The internal layering structure when families of parabolic cyclides are cut through the plane $z=0$. Here $\ell=-4$ and μ ranges from -2 to 6 in steps of 1. For the ranges discussed in the text, the surfaces $\mu=-2$, -1 require $-3\leqslant\vartheta\leqslant 0$ with $-5\leqslant t\leqslant -\sqrt{(\mu/\ell)}$ and $\sqrt{(\mu/\ell)}\leqslant t\leqslant 5$; $0\leqslant\mu\leqslant 4$ require $-3\leqslant\vartheta\leqslant 0$ and $-5\leqslant t\leqslant 5$; $\mu=5$, 6 require $-3\leqslant\vartheta\leqslant -\sqrt{[-(\mu+\ell)/\ell]}$ and $-5\leqslant t\leqslant 5$.

have plotted for the ranges $-3\leqslant\vartheta\leqslant 0$ with $-5\leqslant t\leqslant -\sqrt{(\mu/\ell)}$ and $\sqrt{(\mu/\ell)}\leqslant t\leqslant 5$, while to omit bridges appearing on parabola (3.7) for $\mu=5$, 6 we have used the ranges $-5\leqslant t\leqslant 5$ and $-3\leqslant\vartheta\leqslant -\sqrt{[-(\mu+\ell)/\ell]}$. The full three-dimensional structure can be visualized by including the mirror image of figure 7 in the $z=0$ plane and letting ϑ and t tend to $\pm\infty$. It is clear from figure 7 that we recover figure 6 when we restrict our attention solely to the $z=0$ plane and let ϑ and t tend to $\pm\infty$; the 'gaps' in figure 7 actually close up to form the circles and straight lines of figure 6.

3.2. *The $y=0$ plane*

From symmetry, there is also a parabolic line defect on parabola (3.7) in the xz-plane when $y=0$. From (3.4), $y=0$ whenever one of the following possibilities holds:

$$\text{(i) } t=0, \quad \text{(ii) } t=\pm\infty, \quad \text{(iii) } \vartheta^2=-(\mu+\ell)/\ell. \tag{3.12}$$

Analogous to the $z=0$ case above, for $\mu\leqslant-\ell$, only equations (3.12) (i) and (ii) are relevant. In case (3.12) (i) we have

$$\left.\begin{aligned} x&=\{\mu(\vartheta^2-1)-\ell(\vartheta^2+1)\}(1+\vartheta^2)^{-1},\\ z&=-2\vartheta\mu(1+\vartheta^2)^{-1},\end{aligned}\right\} \tag{3.13}$$

and thus

$$(x+\ell)^2+z^2=\mu^2. \tag{3.14}$$

Hence for $0\leqslant\mu\leqslant-\ell$ we have circles in the xz-plane centred at $(-\ell,0,0)$ of radius μ and parameterized by (3.13) for $-\infty<\vartheta<+\infty$. When $\mu=-\ell$ we come to parabola (3.6)

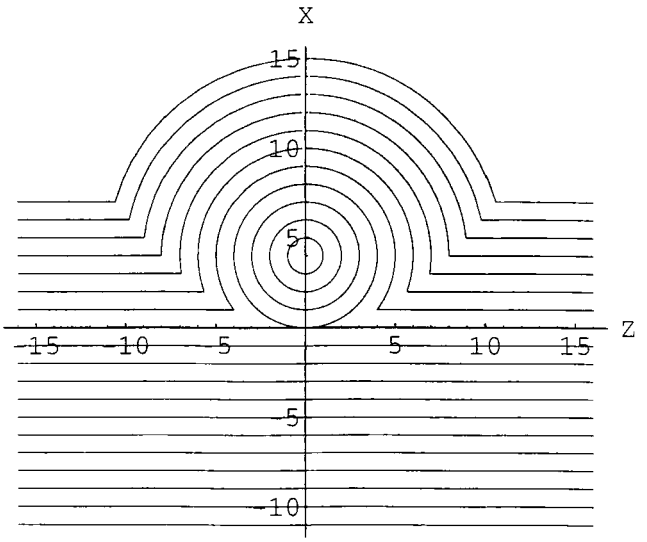

Figure 8. The cross-section of the layers in the xz-plane when $\ell = -4$ and μ ranges from -7 to 11 in steps of 1, the same layers as in figure 6. The parabolic defect (3.3) (or, equivalently, (3.7)) is clearly displayed.

and, as earlier, bridges start appearing for $\mu > -\ell$ whose cusp points lie outside the $y=0$ plane; since bridges are ignored, they do not appear in figure 8. Further, by (3.12) (ii) and (3.4), we must include the straight lines

$$x = \mu + \ell, \quad y = 0, \quad z = 2\ell\vartheta, \quad -\infty < \vartheta < +\infty, \tag{3.15}$$

whenever $\mu \leqslant -\ell$. It now follows that there are the circles (3.14) for $0 \leqslant \mu \leqslant -\ell$ together with the straight lines (3.15) for $\mu \leqslant -\ell$. In the cases when $\mu > -\ell$, equation (3.12) (iii) is possible and bridges start appearing on parabola (3.7). Both equations (3.13) and (3.15) still hold for $\mu > -\ell$, the only difference being that we parameterize for $-\infty < \vartheta \leqslant -\sqrt{[-(\mu+\ell)/\ell]}$ and $\sqrt{[-(\mu+\ell)/\ell]} \leqslant \vartheta + \infty$, to avoid bridges. Figure 8 shows the resulting cross-section in the xz-plane when $y=0$ for the cases where $\ell = -4$ and μ ranges from -7 to 11 in steps of 1, the same layers as considered in figure 6. The maximum and minimum values for ϑ have been set as 2 and -2. The parabolic line defect (3.7) is clearly displayed.

To picture the internal layering in three dimensions near $y=0$, we may slice the family of cyclides along the xz-plane as shown in figure 9 where we only consider the relevant ranges for $t \geqslant 0$. We choose $\ell = -4$ and look at the same layers as in figure 7, namely $\mu = -2, -1, 0, 1, 2, 3, 4, 5, 6$. For $0 \leqslant \mu \leqslant 4$ we have plotted equations (3.4) for $-5 \leqslant \vartheta \leqslant 5$ and $0 \leqslant t \leqslant 3$ while, to omit bridges on parabola (3.7) for $\mu = 5, 6$, we have plotted $0 \leqslant t \leqslant 3$ with $-5 \leqslant \vartheta \leqslant -\sqrt{[-(\mu+\ell)/\ell]}$ and $\sqrt{[-(\mu+\ell)/\ell]} \leqslant \vartheta \leqslant 5$ and for $\mu = -2, -1$ we have the ranges $-5 \leqslant \vartheta \leqslant 5$ and $\sqrt{(\mu/\ell)} \leqslant t \leqslant 3$. The viewing position and parameter ranges are different from those in figure 7 in order to show the layers more perceptively. As before, the full three-dimensional structure includes the mirror image of figure 9 in the $y=0$ plane, letting ϑ and t tend to $\pm\infty$. Figure 8 is recovered from figure 9 by looking at the $y=0$ plane as ϑ and t tend to $\pm\infty$. From figures 6 to 9 the structure of the layers around the parabolic line defects becomes apparent.

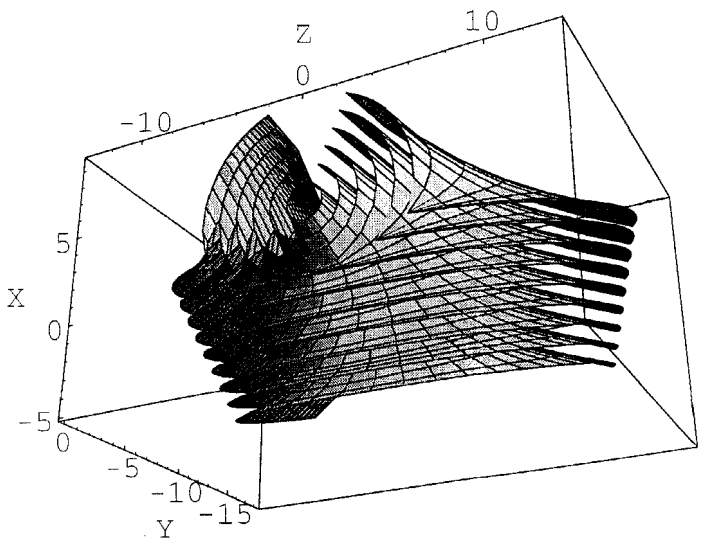

Figure 9. The internal layering structure when families of parabolic cyclides are cut through the plane $y=0$. Here $\ell=-4$ and μ ranges from -2 to 6 in steps of 1, as in figure 7. In this case the viewing position of the layers and the extent of the ranges for ϑ and t are different from those of figure 7 to make the configuration clearer. The surfaces $\mu=-2,\ -1$ require $-5\leqslant\vartheta\leqslant 5$ with $\sqrt{(\mu/\ell)}\leqslant t\leqslant 3$; $0\leqslant\mu\leqslant 4$ require $-5\leqslant\vartheta\leqslant 5$ and $0\leqslant t\leqslant 3$; $\mu=5,\ 6$ require $0\leqslant t\leqslant 3$ with $-5\leqslant\vartheta\leqslant-\sqrt{[-(\mu+\ell)/\ell]}$ and $\sqrt{[-(\mu+\ell)/\ell]}\leqslant\vartheta\leqslant 5$.

4. Discussion

Much of the relationship between parabolic focal-conic defects and liquid crystals has been discussed in Rosenblatt *et al.* [8], who mention, for example, that the cusps which appear are conical at the cyclide surface, having cylindrical symmetry about a line tangent to the parabola on which they lie. One important feature of the cusps is that they become less sharp as $\mu\to\pm\infty$: this is also clear from figures 6 and 8. Examining the behaviour of static solutions near these conical cusps would be of great interest. Although [8] is mainly concerned with the smectic A phase, the appearance of the defects on the parabolas will be similar for other smectic phases, for example, the smectic C* phase. It would also be interesting to examine some of the ideas presented in [8, 10] for the formation of multiple parabolic defects. It may be possible to utilize equations (3.4) and mathematically produce the internal layering structure by suitably intersecting groups of confocal-parabolas and choosing parabolas to match the observed physics. It is straightforward to program (3.4) for computer plots using the results of this paper and then experiment with various options of the parameters.

Kléman [13] has discussed, from energy considerations, Dupin and parabolic cyclides using slightly different techniques to those used here. He mentions two types of parabolic cyclide configuration: his figure 6 (*a*) corresponds to the cyclides filling space as discussed in this paper, while his figure 6 (*b*) considers the parallel layers built up from considering only the bridges. This second configuration can be constructed, for example, from equation (3.4) by setting $\ell<0$ and plotting the bridges based on parabola (3.6) for $\mu\leqslant 0$, where the ranges are $-\infty<\vartheta<\infty$ with $-\sqrt{(\mu/\ell)}\leqslant t\leqslant\sqrt{(\mu/\ell)}$. From approximate calculations of smectic A energies (outside a central core radius) Kléman deduced that this second type of configuration has a higher energy than that of the first type; that is, cyclide layers constructed without bridges are energetically favoured over those consisting solely of bridges. This helps to explain why the layers

depicted in § 3 above have been observed more readily by Rosenblatt *et al.* [8]. Mathematically, it would also be interesting to find out if minimizing the energy (2.3) over a suitable region (not containing defects) with respect to ℓ for the static solution (2.4) could lead to an optimum value of ℓ which minimizes the energy in terms of the elastic constants. The distance between the foci could be measured and is simply $|\ell|$, as can be clearly seen from figures 6 and 8, where $|\ell| = 4$. (For example, in figure 6, $|\ell|$ is the distance between the centre of the circles and the straight line at $x = |\ell| = 4$.) An observed value of $|\ell|$ could then perhaps lead to an evaluation for combinations of elastic constants: in the special case of smectic A, this could perhaps allow a measurement of K_1 (the smectic A phase only has one bulk energy term, namely $\frac{1}{2}K_1(\nabla \cdot \mathbf{a})^2$). As mentioned by Kléman, the main problem to tackle in such an analysis would be the introduction of a core energy near the defects.

The lines of curvature appearing in the three-dimensional plots presented above are actually locally parallel to the surface tangent vectors $\hat{\mathbf{s}}$ and $\hat{\mathbf{t}}$. This means that the static solution given by (2.4) represents the director $\mathbf{c}$ remaining parallel to the lines of curvature running, roughly speaking, along the z-direction when looking at the plot in figure 7 near the origin. Since this solution can only be derived for the first six terms of the smectic energy (2.3), it may be possible to examine the plots presented here in an attempt to find physically meaningful choices for $\mathbf{c}$ which could provide candidates for static equilibrium solutions to the Euler–Lagrange equations for all nine terms in the bulk energy used in the smectic continuum theory.

The author wishes to thank Professor F. M. Leslie for many stimulating discussions on smectic liquid crystals and Professor J. W. Goodby for initially bringing to his attention the relationship between figures 1 and 3 and the experimental observations contained in [4]. Part of this work was carried out under the U.K. SERC funded Smectic Continuum Theory Consortium, coordinated by M. G. Clark at the G.E.C. Hirst Research Centre in Wembley, England.

References

[1] Bouligand, Y., 1980, *Disloc. Solids*, **5,** 300.
[2] Bragg, W., 1934, *Nature, Lond.*, **133,** 445.
[3] de Gennes, P. G., 1974, *The Physics of Liquid Crystals* (Oxford University Press).
[4] Gray, G. W., and Goodby, J. W., 1984, *Smectic Liquid Crystals* (Leonard Hill).
[5] Hartshorne, N. H., and Stuart, A., 1970, *Crystals and the Polarising Microscope*, 4th edition (Edward Arnold), p. 513.
[6] Maxwell, J. C., 1868, *Q. Jl pure appl. Math.*, **9,** 111.
[7] Nakagawa, M., 1990, *J. phys. Soc., Japan*, **59,** 81.
[8] Rosenblatt, C. S., Pindak, R., Clark, N. A., and Meyer, R. B., 1977, *J. Phys., Paris*, **38,** 1105.
[9] Stewart, I. W., Leslie, F. M., and Nakagawa, M., *Smectic Liquid Crystals and the Parabolic Cyclides* (to appear).
[10] Benton, W. J., and Miller, C. A., 1983, *Prog. Coll. polym. Sci.*, **68,** 71.
[11] Hirst, A. E., 1990, *Bull. Inst. Math. Applic.*, **26,** 41.
[12] Hilbert, D., and Cohn-Vossen, S., 1952, *Geometry and the Imagination* (Chelsea Publishing Company), p. 218.
[13] Kléman, M., 1977, *J. Phys., Paris*, **38,** 1511.
[14] Leslie, F. M., Stewart, I. W., and Nakagawa, M., 1991, *Molec. Crystals liq. Crystals*, **198,** 443.
[15] Oseen, C. W., 1933, *Trans. Faraday Soc.*, **29,** 883.
[16] Leslie, F. M., Stewart, I. W., Carlsson, T., and Nakagawa, M., 1991, *Cont. Mech. Thermodyn.*, **3,** 237.
[17] Orsay Group on Liquid Crystals, 1971, *Solid St. Commun.*, **9,** 653.
[18] Forsyth, A. R., 1912, *Lectures on Differential Geometry of Curves and Surfaces* (Cambridge University Press), p. 328.